ANALYSIS OF IMPACT OF MWD INSTRUMENT STRUCTURAL PARAMETERS ON EQUIPMENT RELIABILITY

Huiyuan YU[1]*, Zhongli BAO[2], Yanzuo SONG, Shuyi ZHANG, Jianfeng LIU

This paper investigates the impact of the structural configuration of a typical Measurement While Drilling (MWD) instrument on its sealing performance and vibration characteristics. Finite element models are developed using ANSYS Workbench, considering different barrel distribution schemes and electronic skeleton shaft diameters. The study shows that dividing a long barrel into shorter ones can effectively enhance sealing performance within a certain dogleg severity, with reducing the barrel length to 20% of its original size yielding the best results. The effect of decreasing the electronic skeleton shaft diameter on the overall fatigue life of the instrument initially increases and then decreases, while the short barrel model exhibits a longer fatigue life compared to the original model.

Keywords: Measurement While Drilling (MWD) instrument, sealing performance, dogleg severity, triaxial random vibration, fatigue life

1. Introduction

Advancements in petroleum exploration and drilling have led to increased use of Measurement While Drilling (MWD) systems in directional drilling [1-3]. The complex environment causes interactions between MWD instruments, wellbores, and rock formations, resulting in intricate stress, dynamics, and deformation. Research into MWD operational characteristics and structural improvements is essential. Changes in barrel length affect the instrument's sealing, stability, and drilling efficiency, while both barrel length and electronic skeleton shaft diameter impact vibration fatigue. This paper uses finite element analysis to examine how structural parameters influence the sealing and vibration characteristics of a typical MWD instrument.

Significant work has been done to improve MWD instruments. Reference [4] verifies the main body strength using finite element methods, with optimization ensuring the safety factor meets requirements. Reference [5] identifies stress concentration and tool marks as causes of grouting accidents, with fillet optimization suggested to improve stress distribution. Reference [6] uses response surface simulation and the Box-Behnken method to optimize key stressed

[1] Eng., China Oilfield Services Limited, Hebei 065201, China, e-mail: yuhy8@cosl.com.cn.
[2] Eng., China Oilfield Services Limited, Hebei 065201, China, e-mail: baozhl2@cosl.com.cn.

components. Reference [7] analyzes stress concentration in four drill collar structures and proposes optimization schemes. Reference [8] designs a new MWD shock absorber using vibration theory, enhancing its reliability.

This paper analyzes the impact of barrel length variations on the sealing performance of a typical MWD instrument. The effects of different barrel lengths on the sealing contact surfaces of a typical MWD instrument are analyzed under conditions of dogleg severity of 15°/30 m and 22.5°/30 m [9]. To simulate the fact that the product simultaneously experiences vibrations from three directions in its actual working environment, the interactive effects of triaxial vibration are fully considered. Building upon the analysis of sealing performance, this paper selects an optimized barrel length scheme with superior sealing characteristics, taking a typical MWD as an example to analyze and explore the effects of barrel length and electronic skeleton shaft diameter on its vibration characteristics and fatigue life, so as to provide a theoretical basis for the optimization design of its structure.

The flowchart is shown in Fig. 1.

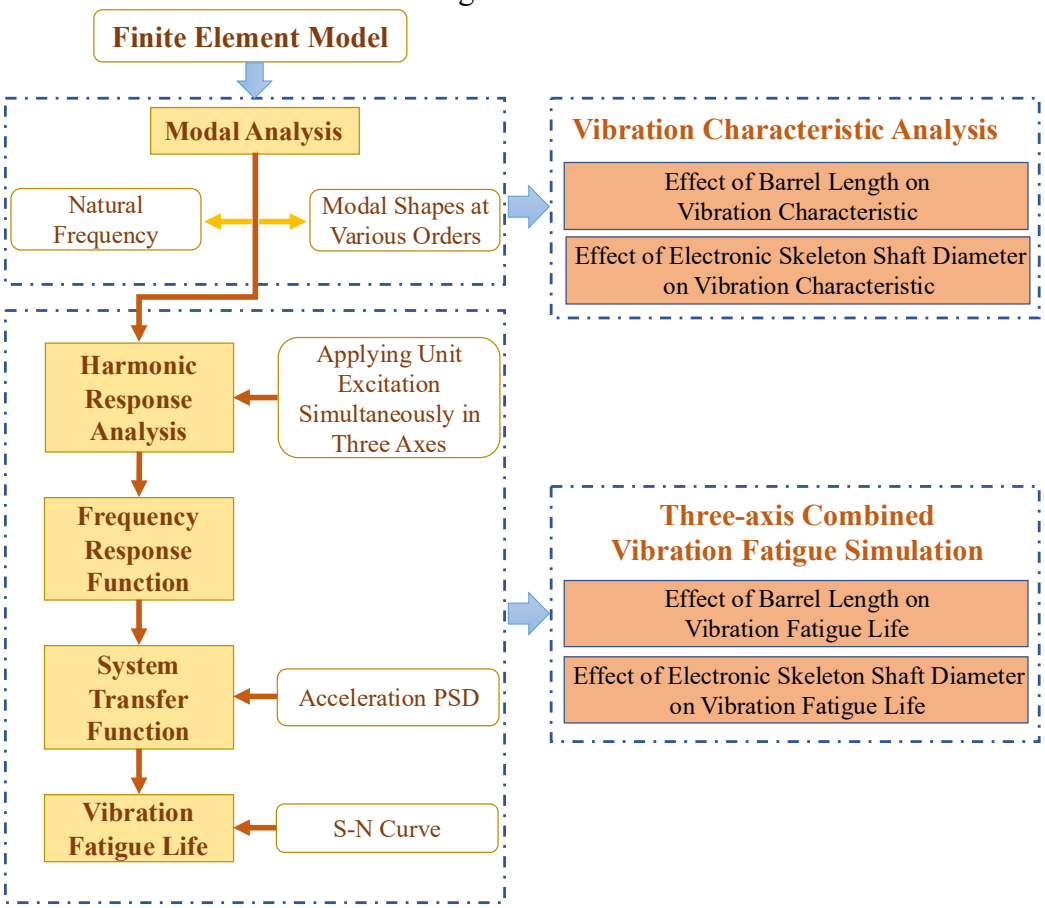

Fig. 1. Flowchart of sealing performance and vibration characterization analysis

2. Theoretical Analysis

2.1. Sealing Theory

The most direct way to assess seal failure is to detect leakage. If leakage is detected, it indicates seal life degradation. Let the seal cavity volume be P and service life be Q, then the allowable leakage rate $[V]$ can be expressed as P/Q, where V is the leakage rate. To ensure the specified service life, the actual leakage V must satisfy: $V \leq [V]$.

The most commonly used method to determine seal failure is the contact equivalent stress criterion. This method compares the stress on the seal contact surface with the internal pressure of the sealed medium to assess whether leakage has occurred. The seal contact minimum stress is denoted as F_{cmin}, and the medium maximum pressure is denoted as F_{max}. For the seal to achieve its sealing function without leakage, it must satisfy the condition: $F_{cmin} \geqslant F_{max}$.

The von Mises criterion, also known as the equivalent stress criterion, is derived from the distortion energy theory.

$$\sigma_M = \sqrt{0.5[(\sigma_1 - \sigma_2)^2 + (\sigma_2 - \sigma_3)^2 + (\sigma_3 - \sigma_1)^2]} \tag{1}$$

This study utilizes the contact equivalent stress criterion to evaluate the relative sealing performance of different barrel length models, which is a more straightforward approach.

2.2. Random Vibration Fatigue Theory

Based on the Miner linear cumulative damage theory, the damage caused by each load stress on the typical MWD instrument is summed up until its fatigue failure. The fatigue damage value of the structure is as follows [10] :

$$D = \sum_{i=1}^{k} D_i = \sum_{i=1}^{k} \frac{n_i}{N_i} \tag{2}$$

D_i is the damage caused by the i th load stress S_i, i=1，2，…，k; n_i is the number of cycles of damage caused by the i th load stress S_i. D is the total damage (when D=1, component fatigue failure); N_i is the fatigue life under the i th load stress S_i.

For the continuous state, the number of stress cycles under the internal stress range (Si, $Si+\Delta Si$) in time T is [11]:

$$n_i = E(P) \times T \times P(S_i) \times \Delta S_i \tag{3}$$

$E(P)$is the expected value of the peak value of the random response signal, T is the time of the random response, and $P(Si)$ is the probability density function of the stress amplitude S_i.

By using the simulation software, combined with the acceleration spectrum, the frequency response function of each axis and the time T, the damage Dx, Dy and Dz of the three axes are obtained respectively based on Miner's theory

(Equation 2). After linear accumulation, the total damage *Ds* of the instrument structure is obtained [12] :

$$D_s = D_x + D_y + D_z \tag{4}$$

where *Ds* represents the cumulative damage across all three axes, each D_i (i=x, y, z) is calculated individually using Equation 2. Fatigue failure occurs when Ds=1, consistent with the failure criterion in Miner's theory.

3. Finite Element Model of MWD Instrument with Simplified Skeleton

3.1. Barrel Length Segmentation

The original MWD instrument model is shown in Fig. 2 (a). This study focuses on how barrel length affects the instrument's sealing performance. In the study of sealing, particular attention is paid to stresses and the contact areas of the end face. Therefore, the complex structure of the electronic skeleton is simplified to smooth cylindrical rods [13] in the finite element analysis process. On the basis of the original model, the long barrel in the middle part of the MWD instrument is divided into segments of different lengths. Three barrel length variants are created by equally subdividing the original long barrel into long, 1/3 short, and 1/5 short barrels, while maintaining the overall axial and radial dimensions. The specific division can be seen in Fig. 2 (b). The sealing performance at the pulse terminal face (between the pulse sleeve and barrel) and vortex terminal face (between the turbine sleeve and barrel) interfaces are analyzed comprehensively.

The original long barrel has an axial length of 4665.00 mm and a inside diameter of 152.5 mm. After subdivision, the single barrel segment lengths are 1542.30 mm, and 920.3 mm respectively. With the 3D models prepared, pre-processing is performed for simplified skeleton finite element analysis.

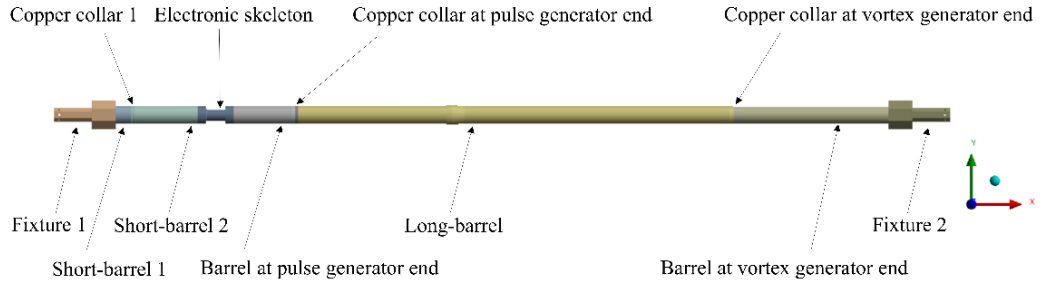

(a) Original model

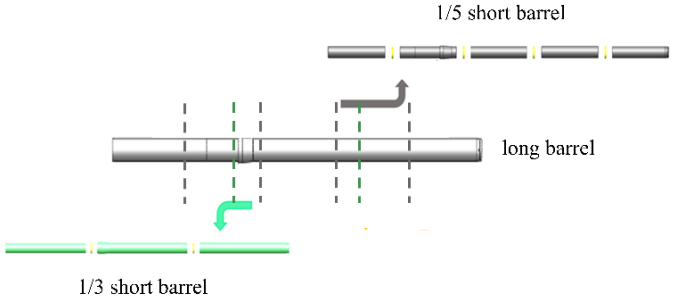

(b) The length division of the barrel

Fig. 2. 3D model building

3.2. Contact Settings and Meshing

The electronic skeleton and barrels use the Incoloy 925 [14] material and the sleeves use the QBe2 alloy [15] material, which are shown in Table 1. Since temperature-equivalent axial preload is applied, a section of the electronic chassis is assigned the "925-T" material with an additional thermal expansion coefficient of 1.32×10^{-5} /°C along the x-axis to facilitate preload application.

Table 1

Material properties

Material	Density (kg/m³)	Young's Modulus (GPa)	Poisson's Ratio	Bulk Modulus (GPa)	Shear Modulus (GPa)	Tensile Strength (GPa)	Yield Strength (GPa)
925	8080	200	0.29	158.73	77.52	0.76	0.97
QBe2	8300	133	0.35	147.78	49.26	1.04	1.04

Due to the complex assembly and contact interactions, face-to-face bonded contacts are defined between the sleeves and barrels at the pulse terminal face and vortex terminal face, while frictionless contacts are set between the electronic skeleton outer surface and barrel inner surface.

To reduce the influence of mesh density on the sealing simulation results, a mesh discretization strategy is formulated prior to the sealing simulations. The specific mesh discretization approach is shown in Table 2. A mesh transition strategy involving progressive refinement towards the sealing faces is selected [16]. The total number of mesh nodes is 1,698,310 with 1,023,609 elements.

Table 2

Mesh division size

Components	Working device	Electronic skeleton	Barrel	Copper ring	Electronic skeleton - copper ring	Barrel-copper ring
Mesh Size	17 mm	15 mm	15 mm	8 mm	2 mm	2 mm

4. Sealing Simulation

4.1. Equivalent Stress

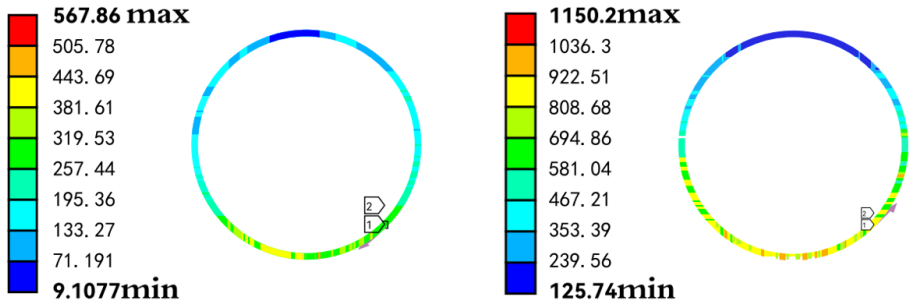

(a) End face stress distribution

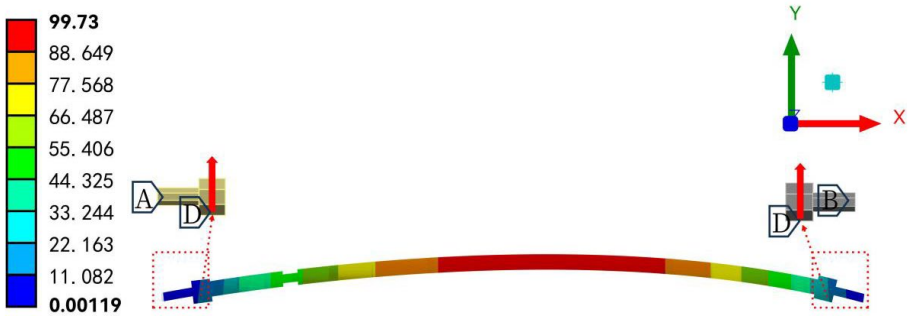

(b) Bending deformation

Fig. 3. Simulation results of sealing

For the MWD instrument, sealing relies primarily on the metal-to-metal contact at the shoulder faces. The condition for ensuring sealing is that the shoulder contact stress exceeds the external pressure. Building on the original MWD instrument model, this study created three barrel length variants by subdividing the long barrel into 1, 1/3, and 1/5 segments while maintaining the original dimensions. Sealing simulations applying a 2200 kN temperature-equivalent axial preload combined with bending moments for 15°/30 m and 22.5°/30 m dogleg severity are performed. Contact equivalent stresses at the pulse terminal face and vortex terminal face boundaries along with total deformations are analyzed.

The end face stress distribution obtained from the three models under the two dogleg severity conditions is similar, with representative results shown in Fig. 3 (a). To apply the bending load, two rigid fixtures were symmetrically installed on both sides of the FEM model, as shown in Fig. 3 (b). Each fixture was fixed to the end face of the structure and had a small hole at the top. Vertical forces were applied through these holes to generate a pure bending moment, simulating the actual dogleg loading scenario. The results show that the maximum displacement occurs

at the middle section of the barrel, which is consistent with theoretical bending behavior.

4.2. Result Analysis

The contact equivalent stress data at the pulse terminal face and vortex terminal face boundaries are extracted from the finite element simulations under 15°/30 m and 22.5°/30 m dogleg severity for the different barrel length models. The results of the two dogleg degrees show similar trends, so only the extracted data at 15°/30 m dogleg degrees are shown in Fig. 4.

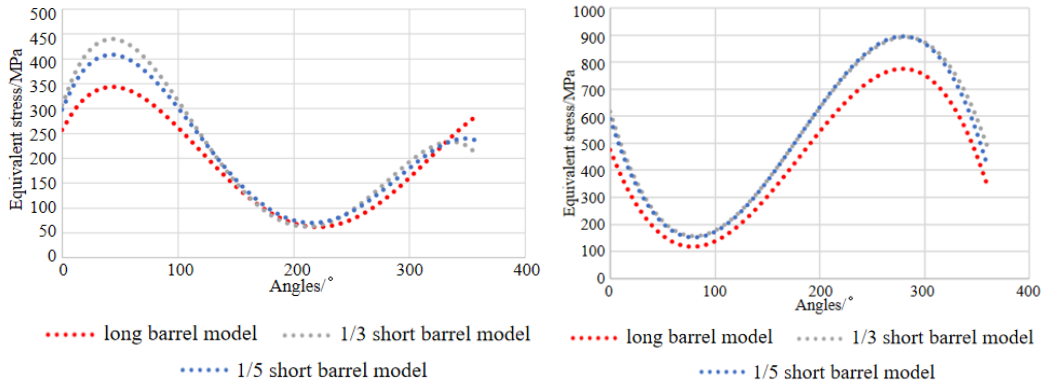

(a) Pulse terminal face (b) Vortex terminal face

Fig. 4. Equivalent force fitting plot

Fig. 4 show that at the same rotational angle, the contact stresses on the pulse terminal face sealing faces differ significantly between models due to barrel length variations, for both 15°/30 m and 22.5°/30 m dogleg severity. Simultaneously, the stress trends exhibit consistent patterns with compression and tension peaks reflecting bending effects, though with varying magnitudes. As shown at the troughs in Fig. 4, the minimum stress values of the short barrel models under both 15°/30 m and 22.5°/30 m dogleg severity are significantly greater than those of the original model. This indicates a notable improvement in sealing performance by shortening the barrel length. However, at the peaks, the maximum stress value of the 1/3 short barrel model is notably greater than that of the 1/5 short barrel model. At this point, the equivalent stress is already substantial, and the focus should be on keeping it far from the yield strength of material to prevent yielding phenomena. Therefore, the 1/5 short barrel model is a preferable choice. The pulse terminal neutral layer at the contact surface of each model is unaffected by external bending loads, and the equivalent stress at this point is only related to axial preload force.

In summary, under both 15°/30 m and 22.5°/30 m dogleg severity, the minimum equivalent stress at the pulse terminal of the 1/5 short barrel MWD model

is greater than the minimum equivalent stress of the original model, significantly enhancing the sealing performance. Moreover, the maximum equivalent stress value is lower than that of the 1/3 short barrel model, keeping it far from the yield strength, making it the optimal choice.

Similarly, Fig. 4 show that the vortex terminal face stress trends mirror those of the pulse terminal face, with compression and tension peaks. Under the 15°/30 m and the 22.5°/30 m conditions, the long barrel has the lowest stresses in the trough of wave, indicating poorer sealing. The other two models exhibit closely matched sealing performance. However, it's worth noting that at this point, the maximum stress values of both short barrel models exceed the yield strength of material, resulting in yielding phenomena in the models.

To facilitate quantitative comparisons, the maximum and minimum contact equivalent stresses around the circumference are tabulated for the pulse terminal face and vortex terminal face, as shown in Table 3.

Table 3

Simulation results of sealing

Model		Long barrel/ MPa	1/3 barrel / MPa	1/5 barrel / MPa
Pulse terminal	15°/30 m	23.13~424.31	10.29~669.17	14.62~582.48
	22.5°/30 m	62.19~530.26	111.21~826.09	100.32~732.72
Vortex terminal	15°/30 m	113.72~891.85	133.14~1139.00	117.09~1090.20
	22.5°/30 m	83.23~1074.70	88.95~1339.00	85.80~1310.70

According to the table data, it can be seen that when the dogleg severity is 15°/30 m, the sealing performance of the short barrel model is better than that of the long barrel model, and the 1/5 short barrel model is the optimal choice; when the dogleg severity is 22.5°/30 m, for the pulse terminal, dividing the long barrel into short barrels improves the sealing performance of the model, but yielding phenomena occur at the vortex terminal.

In summary, the short barrel model can enhance the sealing performance of the MWD instrument within a reasonable dogleg severity, and dividing the long barrel into 5 sections is better. Due to the variable and complex dogleg severity of MWD instrument in practical operations, it is necessary to comprehensively consider the minimum and maximum stress values on the sealing end faces when selecting the optimal barrel length, in order to achieve the best sealing effect under safe conditions.

Considering that the dogleg severity of MWD varies widely in practice, it is necessary to comprehensively consider the equivalent stress values of the outer boundaries of the sealing end faces of each model to achieve better sealing effects under safe conditions when selecting the optimal barrel length.

5. Finite Element Model of MWD Instrument with Electronic Skeleton

The optimal barrel allocation scheme obtained from the previous analysis is adopted, resulting in the construction of a short-barrel electronic skeleton model as Fig. 5 by dividing the long barrel into five segments.

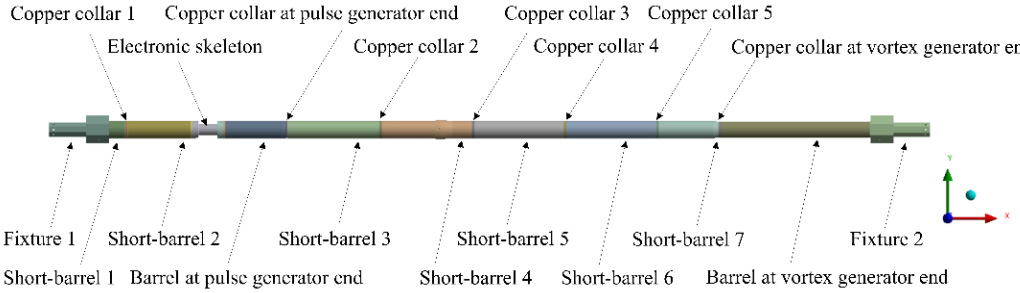

Fig. 5. Short-barrel model of typical MWD instrument

The hollow barrel contains a hollow electronic skeleton. The front and cross-sectional view of the electronic skeleton are shown in Fig. 6. The hollow shaft diameter of the original model electronic skeleton is 48.5 mm. According to the preliminary experiments, it is found that under the action of axial precompression, when the hollow shaft diameter of the electronic skeleton gradually increases to 60.5 mm, the maximum stress continued to decrease. Therefore, five solid models, namely, the hollow shaft diameter of the electronic skeleton d=36.5 mm, 42.5 mm, 48.5 mm, 54.5 mm and 60.5 mm, are created respective.

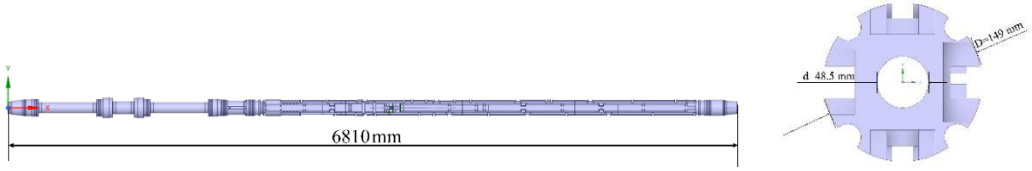

(a) Front view (b) Cross sectional

Fig. 6. Electronic skeleton model

6. Random Vibration Fatigue Analysis of typical MWD Instrument

6.1. Frequency Response Analysis

The main purpose of frequency response analysis is to obtain the frequency-stress transfer function under unit excitation, so as to predict the sustained dynamic characteristics of the structure and verify whether the design can overcome the hazards caused by resonance and fatigue.

Simulation software is used to analyze the frequency response of a typical MWD instrument composed of six structural components, with the left and right tooling ends fixed. The fatigue analysis follows the integrated simulation workflow

shown in Fig. 8, which systematically combines modal analysis, harmonic response characterization, and fatigue damage calculation. In the modal and harmonic response analysis phase (left branch of Fig. 8), a gravitational acceleration of 9.814 m/s² (1g) was applied in the X, Y, and Z directions to simulate static preload effects caused by the instrument's self-weight, ensuring accurate natural frequency predictions under realistic structural stiffness conditions. According to the pre-experiment, the 15th-order natural frequency of the typical MWD instrument doesn't exceed 200 Hz. Therefore, the frequency band is defined as 0–300 Hz, and the damping ratio is set to 0.02. As shown in Fig. 7 (a), the responses in the Y and Z directions exhibited strong similarity, whereas the amplitude in the X direction was significantly smaller. Consequently, the Y-direction response (Fig. 7 (b)) was selected for comparative analysis.

In the fatigue analysis phase (right branch of Fig. 8), a dynamic power spectral density (PSD) curve derived from the COSL enterprise standard was applied in nCode. This curve rigorously decouples static prestress effects (modeled via 1g) from operational dynamic loads, enabling fatigue damage accumulation based on Miner's rule and SN curves. This phased methodology ensures compliance with industry standards while maintaining fidelity to field-measured vibration characteristics.

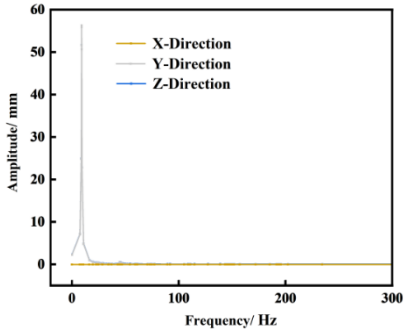

(a)

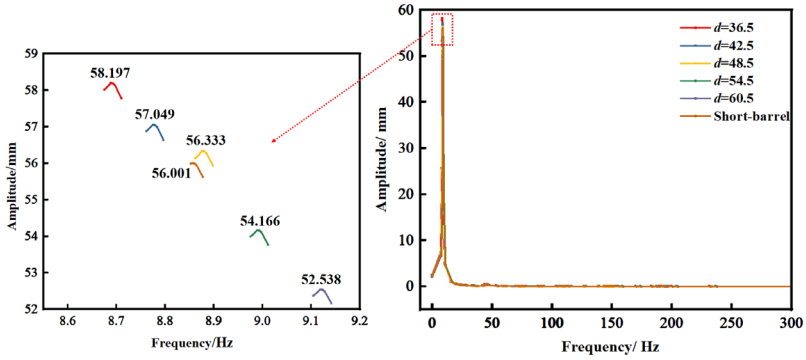

(b)

Fig. 7. Frequency response of typical MWD instrument

It can be seen from Fig. 7 (b) that the displacement frequency response curves of the typical MWD instrument with different structural parameters almost coincided, but with the increase of the shaft diameter of the electronic skeleton, the maximum vibration amplitude gradually decreases and the corresponding frequency gradually increases. When the shaft diameter of the electronic skeleton is 60.5 mm, the maximum vibration amplitude reaches the minimum and the corresponding frequency is the maximum. Compared with the original model, the maximum vibration amplitude and corresponding frequency of the short-hold barrel model are smaller.

6.2. Random Vibration Fatigue Life Analysis

The frequency response function of the typical MWD instrument is transferred to the fatigue life analysis software, and the simulation flow chart is shown in Fig. 8. According to the frequency response, the amplitude concentration appears in 0-15 Hz, the random vibration power spectral density developed by the enterprise according to the actual project is simultaneously loaded in the X, Y and Z directions, as shown in Fig. 9 (a). The S-N curve of the material is automatically fitted by the software, and the stress combination method of the relative maximum principal stress and the Goodman mean stress correction method are used to simulate the three-axis combined vibration fatigue of the overall instrument for the six models respectively. The random vibration fatigue life profile of the typical MWD instrument is obtained.

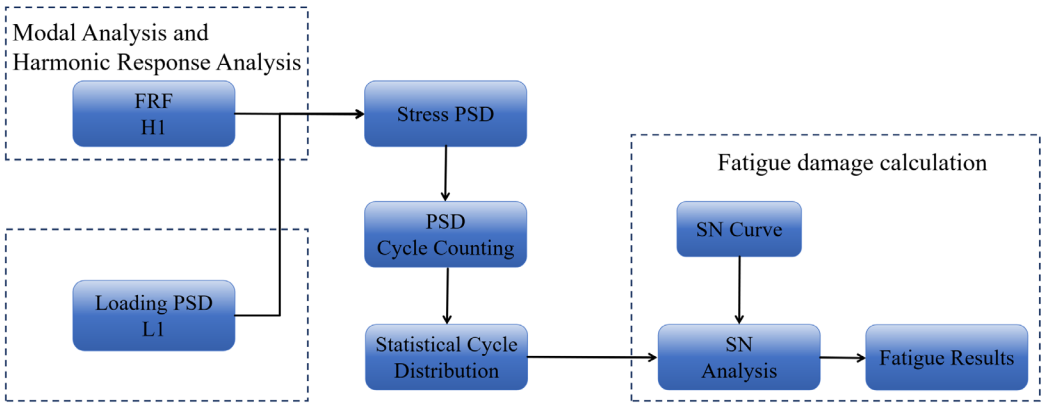

Fig. 8. Simulation flow chart

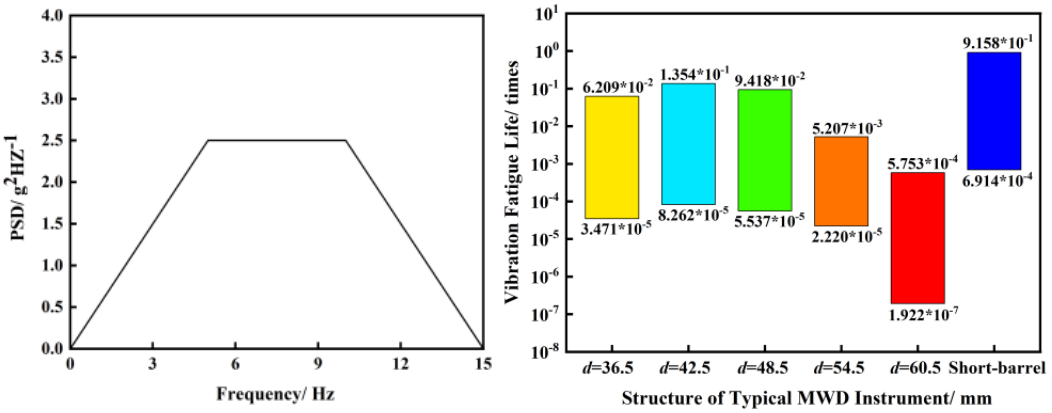

(a) PSD (b) Vibration fatigue life

Fig. 9. PSD and results of vibration fatigue life analysis

The random vibration fatigue life distribution of the six models are roughly the same. The fatigue life of the whole instrument is small in the variable fillet, the left section of the short barrel, the middle section of the long barrel and the stress concentration area of the electronic skeleton, which need to be paid attention to.

The fatigue life of the area that need to be focused on is extracted, as shown in Fig. 9 (b). It can be found that the fatigue life of the typical MWD instrument increases with the decrease of the electronic skeleton shaft diameter, reaching the maximum value when the electronic skeleton shaft diameter d=42.5 mm. However, when the electronic skeleton shaft diameter is reduced from 42.5 mm to 36.5 mm, the fatigue life decreases instead. Compared with the original model, the random vibration fatigue life of the short barrel is longer.

7.Conclusions and Discussions

This study employs finite element simulation to analyze the impact of the MWD instrument structure on its sealing performance and vibration characteristics, with the following conclusions:

(1)The short barrel model can enhance the sealing performance of the MWD instrument within a reasonable dogleg severity, and reducing the barrel length to 20% of its original size yielding is better.

(2)The natural frequency decreases when the barrel length is shortened or the shaft diameter of electronic skeleton is decreased. When the shaft diameter increases by about 20%, the natural frequency is maximum, and the risk of resonance is minimal.

(3)The fatigue life is relatively small at the variable fillet, the left section of the short barrel, the middle section of the long barrel and the stress concentration area of the electronic skeleton. When the length of the barrel become shorter, the

vibration fatigue life increases. Moreover, the vibration fatigue life reaches the maximum value when the shaft diameter is reduced by about 10%.

Due to the limitations of the model, the discussion in this paper is only based on the typical MWD instrument, and further research is needed to determine whether the conclusions obtained are universal. This paper provides a direction for the subsequent discussion and has certain value.

Acknowledgements

This study is financially supported by "China National Offshore Oil Corporation Scientific and Technological Specialized Measurement and Recording Test Key Technology and Equipment" with the project numbers of KJGG-2022-1401. This study is financially supported by "Science and Technology Project of CNOOC Oilfield Services Co. Model 675 Logging Technology and Equipment for Drill Followers" with the project numbers of YJB22YF003.05.

REFERENCES

[1]. *Z. Wang, Z. Li* Application of Measurement While Drilling Technology in Petroleum Exploration and Development in China. Petrochemical Technology, **vol.25, no.12**, 2018, 118+84.

[2]. *Z. Wu, S. Deng, X. He, et al.* Numerical simulation and dimension reduction analysis of electromagnetic logging while drilling of horizontal wells in complex structures. Petroleum Science, **vol.17, no.3**, 2020, pp. 645-657.

[3]. *L. Wang, Y. Fan, C. Yuan, et al. Zhao.* Selection criteria and feasibility of the inversion model for azimuthal electromagnetic logging while drilling(LWD). Petroleum Exploration and Development, **vol.45, no.5**, 2018, pp. 974-982.

[4]. *H. Hou, Z. Yu, S. Liao, et al.* Finite Element Simulation and Optimization Design of Main Body Structure of Measurement While Drilling Instrument. Oil Tubing and Instrumentation, **vol.9, no.3**, 2023, 39-41+45.

[5]. *C. Qin, H. Lu, Y. Zhu, et al.* Analysis of Downhole Leakage Failure and Structural Optimization of a Certain Cover Plate Measurement While Drilling Instrument. Drilling Engineering, **vol.50, no.2**, 2023, pp. 39-46.

[6]. *X. Wang, L. Xian, L. Chen, et al.* Optimization Design of Stress Components of Coal Mine Drilling Measurement While Drilling Ultrasonic Imaging Instrument Based on Response Surface Method. China Safety Science Journal, **vol.17, no.7**, 2021, pp. 97-102.

[7]. *Y. Feng, Z. Bao, H. Yu.* Finite Element Analysis and Optimization of Drill Hole Slot Structure. China Offshore Oil and Gas, **vol.25 no.4**, 2013, pp. 38-41.

[8]. *M. Yan, X. Liu, Y. Wei, et al.* Structural Design and Research on Vibration Reducer of MWD Measurement While Drilling Instrument. Petroleum Instruments, **vol.18, no.5**, 2014, 14-17+20+7-8.

[9]. *Dykstra M. W, Chen D. C. K, Warren T.M.* Drillstring component mass imbalance: a major source of downhole vibrations. SPE Drill. Completion, pp. 234 – 241.

[10]. *Y. Wang, S. Yan, J. Zhang, et al.* Simulation and Optimization of Fatigue Life of Electric Commercial Vehicle Frame. Mechanical Science and Technology, **vol.42, no.5**, 2023, pp. 673-678.

[11]. *P. Nie, Z Zhong.* Failure Analysis and Optimization Design of Brake Valve Bracket for Light Truck. Modern Manufacturing Engineering, 2019(07): pp. 60-65.
[12]. *C. Chen, G. Yang, S. Xiao, et al.* Structural Optimization of Gearbox Casing Based on Fatigue Life Prediction. Mechanical Strength, **vol.43, no.2**, 2021, pp. 447-452.
[13]. *J. Zhang, L. Duan, H. Wang.* Modal Analysis of Drill Rod Vibration in Coalfield Geological Exploration Based on ANSYS. Coal Science and Technology, **vol.37, no.8**, 2009, pp. 64-66.
[14]. *S. Sujai, K. Devendranath Ramkumar.* Microstructure and Mechanical Characterization of Incoloy 925 Welds in the As-Welded and Direct Aged Conditions. Journal of Materials Engineering and Performance, vol. 28, 2019, pp. 1563 – 1580.
[15]. *Z. Li , Y. L. Jia , N. Tang , et al.* A novel laminate combined with elasticity and damping. Journal of Materials Processing Technology, vol. 182, 2007, pp. 1-5.
[16]. *P. Zhang, H. Xiong, X. Jiang, et al.* A review of large-scale mesh model simplification and multi-resolution techniques. Journal of Computer-Aided Design and Graphics, **vol. 4**, 2010, pp. 559-568.